Remote Sensing of Environment 113 (2009) S25–S37

Contents lists available at ScienceDirect

Remote Sensing of Environment

journal homepage: www.elsevier.com/locate/rse

Interpretation of snow properties from imaging spectrometry

Jeff Dozier [a,*], Robert O. Green [b], Anne W. Nolin [c], Thomas H. Painter [d]

[a] Donald Bren School of Environmental Science and Management, University of California, Santa Barbara, USA
[b] Jet Propulsion Laboratory, California Institute of Technology, USA
[c] Department of Geosciences, Oregon State University, USA
[d] Department of Geography, University of Utah, USA

ARTICLE INFO

Article history:
Received 16 September 2006
Received in revised form 11 June 2007
Accepted 27 July 2007

Keywords:
Snow
Remote sensing
Imaging spectrometry

ABSTRACT

Snow is among the most "colorful" materials in nature, but most of the variability in snow reflectance occurs beyond 0.8 μm rather than in the visible spectrum. In these wavelengths, reflectance decreases dramatically as the snow grains evolve and grow, whereas in the visible spectrum snow reflectance is degraded by contaminants such as dust, algae, and soot. From imaging spectrometer data, we can estimate the grain size of the snow in the surface layer, and thereby derive spectral and broadband albedo. We can also estimate the fraction of each pixel that is covered by snow, the liquid water content in the surface layer, and the amount of radiative forcing caused by absorbing impurities. Estimates of fractional snow-covered area and albedo dramatically improve the performance of spatially distributed snowmelt models that include net solar radiation as an input value, most significantly in locations and at times where incident solar radiation is high and temperatures low. Experience with imaging spectrometer data has allowed extension of the fractional snow-cover and albedo estimates to multispectral sensors, particularly MODIS, the Moderate-Resolution Imaging Spectroradiometer.

1. Introduction

What is there to say about the "color" of snow? In the visible part of the spectrum clean, deep snow is bright and white, irrespective of the size of the grains. Beyond the visible wavelengths in the near-infrared and shortwave-infrared, however, snow is one of the most colorful substances in nature. Newly fallen snow usually has a fine grain size, but metamorphism and sintering throughout the winter and spring increase the grain size and reduce reflectance in wavelengths beyond about 0.8 μm.

This behavior of snow is important to the snowpack's energy balance, because the reduced albedo often occurs in the spring and summer as the incoming solar radiation becomes greater, and also to remote sensing of snow properties. Estimating properties for hydrologic and climate models from imaging spectrometer data is best done through an understanding of the relationship between snow's physical properties and the resulting electromagnetic signal.

Initially, imaging spectrometers mainly focused on identification of surface materials from the wavelength position of known absorption bands. The heritage for the work on snow began with the use of the depth of absorption features, rather than their wavelength position, to infer some geophysical property of the absorbing substance. The primary example of such work is the retrieval of column-integrated atmospheric water vapor and liquid water in vegetation (Gao & Goetz, 1990). Successful estimates depend on careful calibration of the sensor, in terms of the wavelength positions of the bands and the radiometry (Green, 2001).

We review the state of knowledge for estimating the following properties from imaging spectrometry: fractional snow-covered area, snow albedo as affected by grain size and absorbing impurities (dust and red algae), and snow wetness in the near-surface layer. We also describe the application of methods developed with imaging spectrometers to multispectral sensors, specifically MODIS, the Moderate-Resolution Imaging Spectroradiometer, whose ability to image Earth's surface daily enables the use of snow-covered area and albedo in models. Some of the results we review have been published in the journal literature, but some have appeared only in conference papers and presentations. Finally, we briefly examine some research issues.

1.1. Implications of snow albedo variability for the energy balance of the snowpack

Snow evolves after it falls. Long before radiative transfer in snow was understood, energy balance data had shown age-related decrease in snow's albedo, leading to the use of empirical decay functions based on age (U.S. Army Corps of Engineers, 1956) or on accumulated melt (Molotch & Bales, 2006). More recent work has addressed the development of a physical model for albedo evolution, based on

* Corresponding author.
E-mail addresses: dozier@bren.ucsb.edu (J. Dozier), Robert.O.Green@jpl.nasa.gov (R.O. Green), nolina@science.oregonstate.edu (A.W. Nolin), painter@geog.utah.edu (T.H. Painter).

0034-4257/$ – see front matter © 2009 Elsevier Inc. All rights reserved.
doi:10.1016/j.rse.2007.07.029

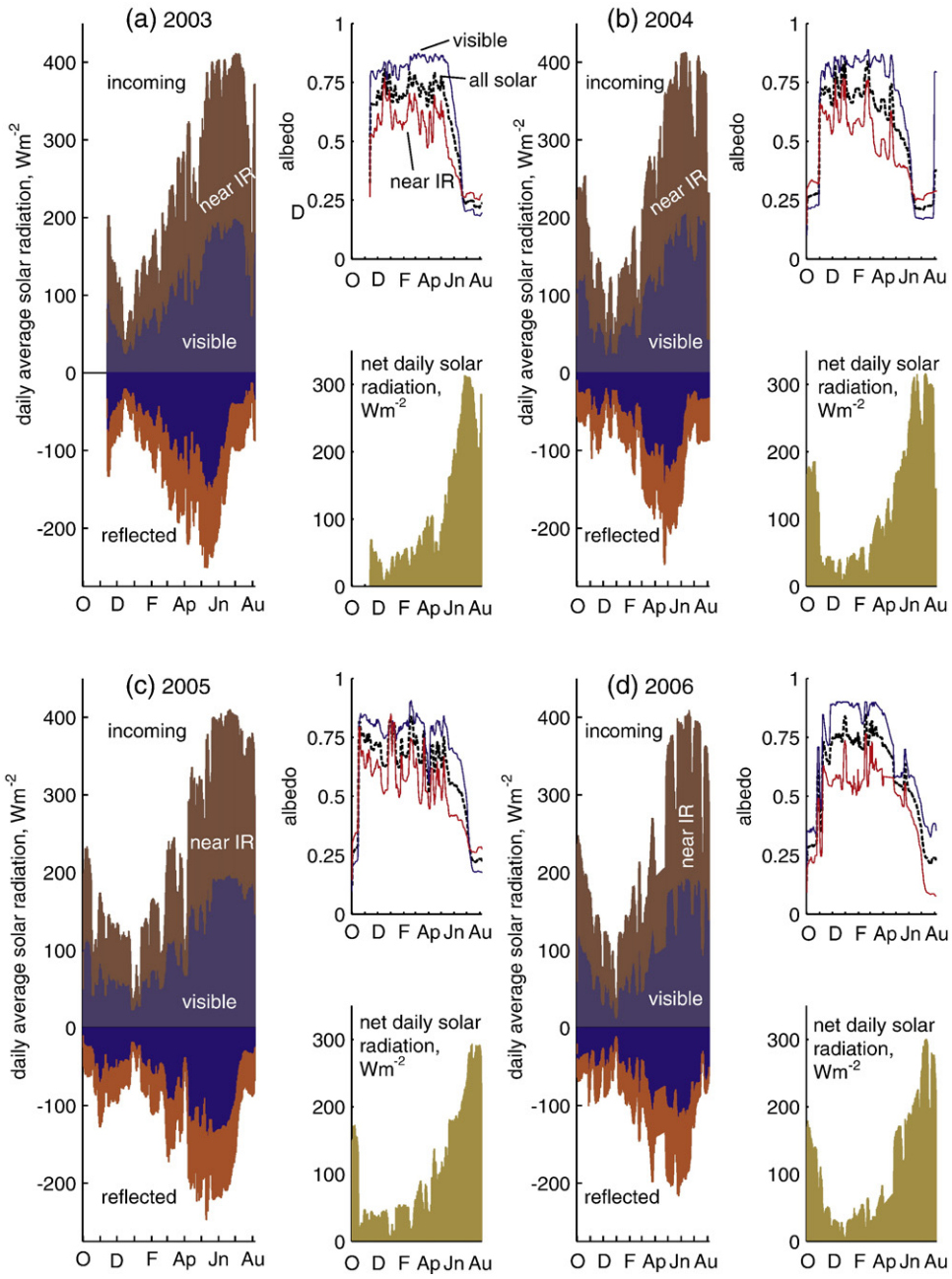

Fig. 1. Field measurements of broadband albedo at Mammoth Mountain in the Sierra Nevada for (a) 2003, (b) 2004, (c) 2005, (d) 2006. For each year, the three graphs show incoming and reflected solar radiation in the visible and near-infrared wavelengths, albedo for the solar spectrum and for the visible and near-infrared, and net solar radiation. All radiation values are daily averages in Wm^{-2}.

diffusion of the water molecules in snow to reduce the specific surface area of the grains (Flanner & Zender, 2006).

We see this albedo decay in the field data. Fig. 1 shows incoming and reflected radiation data for four years at Mammoth Mountain, a high-altitude, mid-latitude station in the Sierra Nevada. Incoming solar radiation increases through the spring because of higher solar elevation and longer days. However, the progressive decrease of broadband albedo causes the net solar radiation to increase more than the incoming radiation.

We see similar albedo decay at high latitudes. In Greenland, for example, both satellite and field measurements show that at low elevations broadband albedo decreases in the early part of the summer, whereas at higher elevations the albedo reduction occurs in mid- to late summer (Stroeve et al., 2005).

Although incoming solar radiation from the Sun peaks in the visible part of the spectrum, about half of that incoming radiation is at wavelengths greater than 0.7 μm. Convolving the incoming radiation with snow's spectral albedo leads to the spectral distribution of net radiation that Fig. 2 shows. In clean snow, the preponderance of the absorbed solar radiation occurs at wavelengths greater than 1 μm, especially for coarse grains.

1.2. Relationship between snow properties and spectral reflectance

A scattering model for any granular medium has two sets of input parameters: the wavelength-dependent complex index of refraction of the constituent materials, and the distribution of the sizes and shapes of the scattering elements. In addition to the snow grains themselves, the

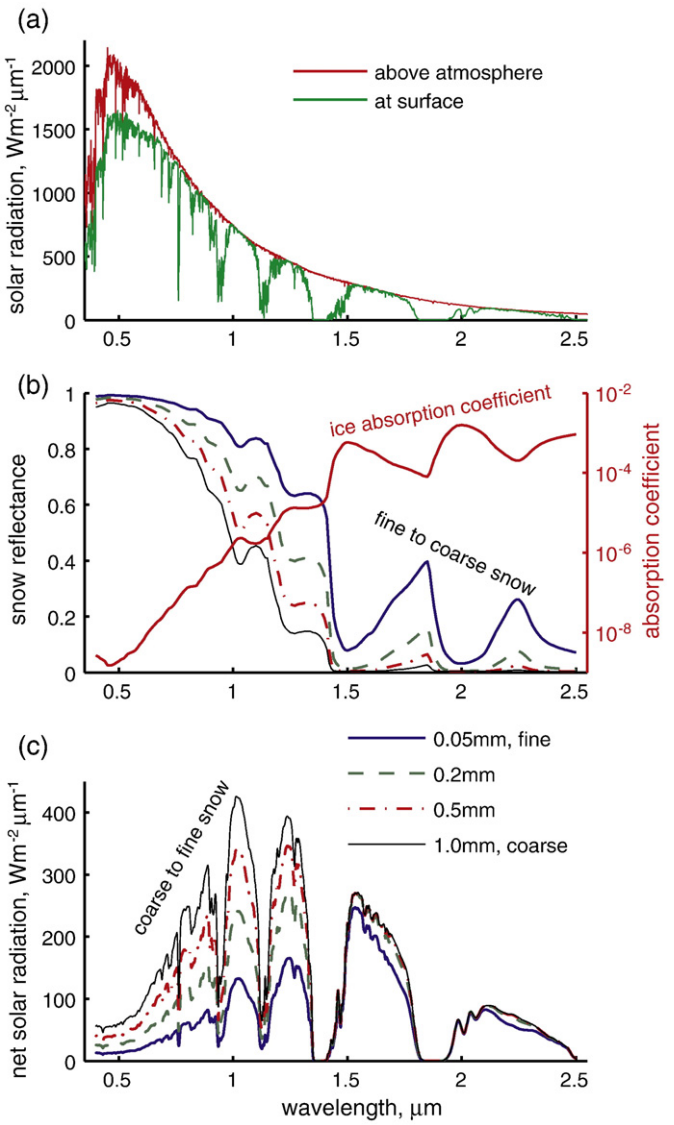

Fig. 2. (a) Spectral distribution of solar irradiance above the atmosphere and at Earth's surface on a 37° slope facing the Sun at a latitude and solar geometry where atmospheric path length is 1.5 (Gueymard, 2004). (b) Spectral reflectance of pure, deep snow for a range of grain sizes (Wiscombe & Warren, 1980), with the absorption coefficient of ice on the right-hand axis. (c) Spectral distribution of net solar radiation of snow for a range of grain sizes, derived from (a) and (b); the solar radiation value from (a) is smoothed to about 0.01 µm spectral resolution.

snowpack sometimes contains liquid water and absorbing impurities such as dust, soot, or algae. Warren (1982) reviewed the theory of snow reflectance, based on the optical properties of the constituents and multiple scattering calculations with a radiative transfer model. Dozier and Painter (2004) reviewed the application of our understanding of these radiative properties to remote sensing of snow in mountainous areas. The problem in imaging spectrometry is to use measurements in specific wavelength regions to estimate the physical properties of the snow, and then to use these estimated properties to model spectral reflectance and broadband albedo.

1.2.1. Grain size

Fig. 3 shows that in snow, the snow grains are often nearly spherical, and can therefore be represented in scattering models as equivalent spheres with the same surface-to-volume ratio. Scattering properties of nonspherical grains can be mimicked as collections of spheres (Grenfell & Warren, 1999) when determining radiative fluxes.

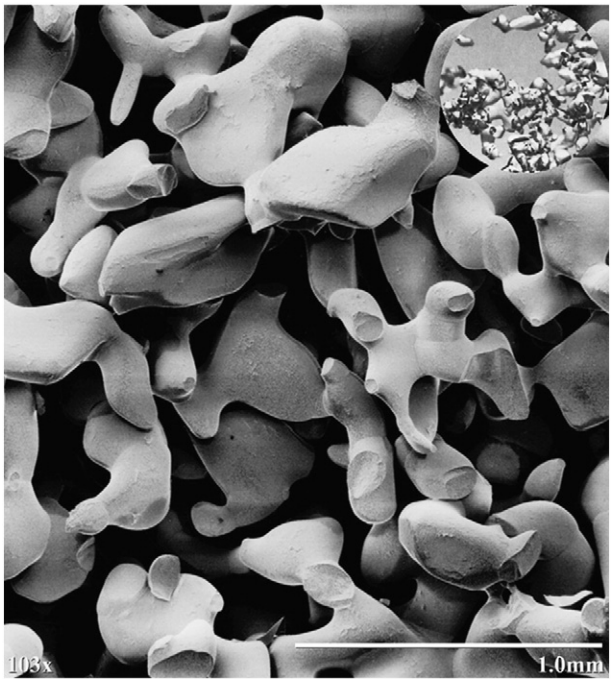

Fig. 3. Scanning electron microscope image of pure snow showing the rounded shape of the bonded grains, with a 1 mm scale line. The circular image in the upper right is from a conventional microscope. The snow sample was collected by Walter Rosenthal at Mammoth Mountain in the spring of 2004 and imaged in the microscope at UC Santa Barbara within 24 h . Walter died 06 April 2006 while rescuing two ski patrollers who had fallen into a collapsed hole in the snow created by a volcanic vent. Additional detailed information on this sample collection is unavailable.

The *broadband albedo* is the spectral reflectance convolved with the incoming solar irradiance. To account for angular effects and the spectral differences between direct and diffuse irradiance, we sometimes distinguish between a *direct* albedo for direct irradiance and a *diffuse* albedo for diffuse irradiance. Fig. 4 shows the relationship between grain size and broadband albedo for direct irradiance, segmented into the visible and near-infrared parts of the spectrum, using typical spectral distributions of solar irradiance for clear skies.

1.2.2. Effect of liquid water

Wet snow's reflectance is subtly different than that of dry snow, but the effect is often misunderstood and the literature is replete with

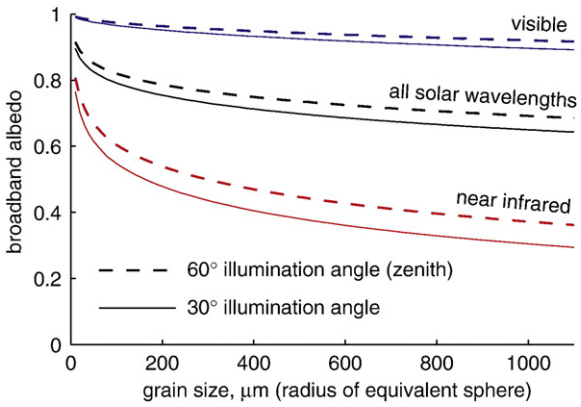

Fig. 4. Relationship between grain size (optically equivalent sphere) and broadband albedo for direct irradiance at 30° and 60° illumination angles (from zenith) for the visible and near-infrared parts of the solar spectrum and the whole solar spectrum. Many Mie scattering and multiple scattering calculations are needed to generate the figure, but the curves can be fit with an equation of the form $R(\theta) = 1 - A(\theta)r^{B(\theta)}$. Table 1 gives values for the A and B coefficients for $\theta = 30°$ and 60°.

Table 1
Coefficients in the equations that fit the curves in Fig. 4.

	$\theta = 30°$		$\theta = 60°$	
	A	*B*	*A*	*B*
Visible	0.0040	0.4730	0.0029	0.4791
All solar wavelengths	0.0765	0.2205	0.0648	0.2258
Near-infrared	0.2025	0.1791	0.1689	0.1906

incorrect statements about why wet snow is darker than dry snow. In the wavelengths of the solar spectrum, there is little difference between the absorption coefficients for ice and water (Wiscombe, 2005). Therefore, the main effect of liquid water in snow is that it causes the grains to form clusters (Colbeck, 1979), which behave optically as larger grains, so broadband albedo decreases when the snow is wet because of the clusters and not because of liquid water per se. However, the absorption features of ice mimic those of water with a slight shift toward longer wavelengths, so at fine spectral resolution there is a similar shift in the reflectance between wet and dry snow (Green et al., 2006).

1.2.3. Effect of dust and algae

Fig. 5 shows field measurements of dirty snow in the San Juan Mountains, where the source of the dust is the deserts of the Colorado Plateau of Utah, Arizona, and New Mexico, and snow with red algae (*Chlamydomonas nivalis*) in the Sierra Nevada. In both cases, the reflectance in the visible spectrum is much lower than for clean snow; in the snow with red algae, chlorophyll absorption features are present.

Dust storms often deposit radiatively absorbing dust on the snowpack in many mountain ranges. Winter and spring storms entrain absorbing dust from desert regions and redistribute optically thick layers to the snow cover as both wet and dry deposition. Radiative transfer theory suggests that dust would decrease spectral reflectance mainly in the visible wavelengths (Warren & Wiscombe, 1980). However, Fig. 5 shows that dirty snow has lower reflectance than clean snow at longer wavelengths too. Apparently, the absorption by the dust particles also increases grain size though local microscale metamorphism. For these two reasons, the radiative effects of desert dust significantly increase the solar radiation absorbed by the snowpack (Painter et al., 2007).

Once snow becomes wet, red algae (*Chlamydomonas nivalis*) that spend the winter season in the underlying soil migrate to the surface, where they photosynthesize and deploy their carotenoid pigments that give their red coloring. Although the algae blooms generally have a more heterogeneous concentration than dust, they also can lower the albedo in the visible wavelengths, but generally not at the scale of whole slope segments (Painter et al., 2001).

2. Snow properties derived from imaging spectrometry

2.1. Imaging spectrometry data sources

Most of the analyses presented herein use the AVIRIS instrument (Green et al., 1998) as the main source of data. The Airborne Visible/Infrared Imaging Spectrometer (AVIRIS) detects upwelling radiance in 224 contiguous spectral channels within the wavelength range 0.37 to 2.51 μm, with a spectral sampling of 10 nm. Normally AVIRIS flies on the ER-2 at ~ 20 km elevation. Images have a 10.5 km swath width and up to 800 km image length. The spatial resolution is nominally 20 m × 20 m when the surface is at sea level, but is 16–17 m when surface elevations are 3000–4000 m. On occasions, AVIRIS flies in a Twin Otter aircraft at about 4000 m altitude, so spatial resolution is 1–2 m depending on the elevation of the surface.

One set of results presented here uses data from Hyperion (Pearlman et al., 2003), the first Earth-looking imaging spectrometer on a satellite. Flying on EO-1, Hyperion provides images with 220 spectral bands from 0.4 to 2.5 μm with 30 m spatial resolution. The instrument images a 7.5 km × 100 km land area per image. Originally flying in tandem with Landsat 7, the mission is now using fuel to move to lower orbit in a controlled way while maintaining the equatorial crossing time of 10AM. EO-1 could operate until 2011, when all its fuel will be expended.

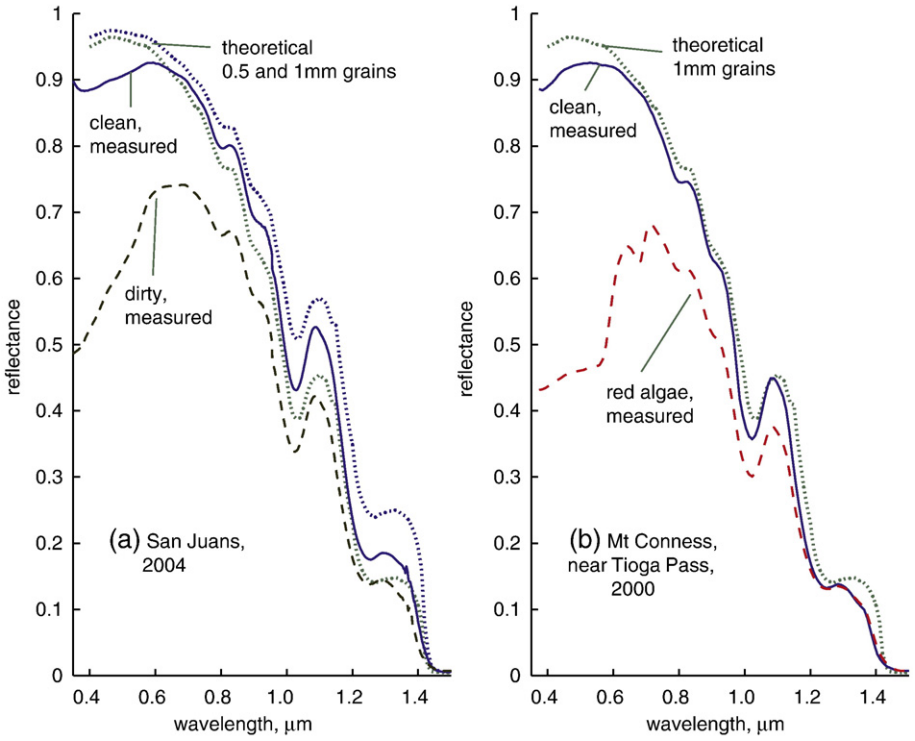

Fig. 5. Field-measured spectral reflectance of: (a) dirty snow in the San Juan Mountains (Painter et al., 2007); and (b) snow with red algae (*Chlamydomonas nivalis*) in the Sierra Nevada (Painter et al., 2001).

2.2. Snow albedo

In the near-infrared and shortwave-infrared parts of the solar spectrum, snow reflectance is primarily sensitive to grain size (Wiscombe & Warren, 1980). Conversely, in the visible part of the spectrum, snow reflectance is less sensitive to grain size but decreases if absorbing materials—dust, soot, or algae—are present or if the snowpack is shallow (Warren & Wiscombe, 1980).

The conventional way to estimate broadband albedo of a spectrally reflecting surface material involves four steps: estimating the at-satellite radiance using calibration data, correcting this measurement for atmospheric scattering and absorption to estimate surface radiance at the measured wavelengths, conversion of these measurements to narrowband albedo, and then estimation of broadband albedo from the measurements at some suite of wavelengths. Each step in this process involves error: perhaps 2–5% in the at-satellite radiance depending on the quality of the calibration, certainly at least 5% in the atmospheric correction, possibly as large as 10% in the conversion to narrowband albedo, and then again another 10% in estimating broadband albedo.

A more robust approach relies on the radiative transfer model of spectral albedo based on the snow's physical properties, and uses the measurements from an imaging spectrometer to estimate those physical properties (Nolin & Dozier, 2000). The method relates an ice absorption feature, centered at $\lambda = 1.03$ μm, to the optically equivalent snow grain size. Because the interpretation is based on the area—not depth—of the absorption feature scaled to absolute reflectance, the method is insensitive to instrument noise and does not require a topographic correction. The area of the absorption feature is the difference between the continuum reflectance R_c and the snow's reflectance R_s, integrated over the wavelengths of the absorption band:

$$A_b = \int_\lambda \frac{R_{c\lambda} - R_{s\lambda}}{R_{c\lambda}} d\lambda \quad (1)$$

Fig. 6 shows the theoretical and field-measured relationships between grain size and the scaled area of the absorption feature. Nolin and Dozier (2000) show persuasive experimental results comparing field measurements and AVIRIS estimates over a range of environments and grain sizes, from fine winter snow to coarse melting snow.

2.3. Fractional snow-covered area

Snow-covered area in alpine terrain often varies at a spatial scale finer than that of the ground instantaneous field-of-view of the remote sensing instrument. This spatial heterogeneity poses a mixed-pixel problem in that the sensor may measure radiance reflected from snow, rock, soil, and vegetation. To use the snow characteristics in distributed hydrologic models and high-resolution regional climate models, we must therefore map snow-covered area at subpixel resolution in order to accurately represent its spatial distribution (Nolin et al., 1993). Spectral mixture analysis is a method of inverting data from imaging spectrometers or multispectral sensors to enable mapping surface constituents at subpixel scale. *Linear* spectral mixture analysis is based on the assumption that the radiance measured at the sensor is a linear combination of radiances reflected from individual surfaces, *endmembers*, whose spectral signatures are unique and well separated above a random image noise level (Sabol et al., 1992). A set of simultaneous equations for N endmembers, one for each wavelength band, results:

$$\overline{R_\lambda^{(p)}} = \sum_{j=1}^{N} F_j R_\lambda^{(j)} + \varepsilon_\lambda \quad (2)$$

$\overline{R_\lambda^{(p)}}$ is the pixel-averaged reflectance at wavelength λ. F_j is the fractional coverage within the pixel of endmember j, $R_\lambda^{(j)}$ is the reflectance of endmember j at wavelength λ, and ε_λ is the spectral residual. Given measurements of $\overline{R_\lambda^{(p)}}$ in M wavelength bands, one normally solves for the F_j values by minimizing RMSE $= \left(\frac{1}{M}\sum_{\lambda=1}^{M} \varepsilon_\lambda^2\right)^{1/2}$, although other minimization criteria can be used.

Given snow's physical characteristics such as grain size and amount and composition of impurities, a snow endmember can be chosen. The concept of multiple endmember spectral mixture analysis

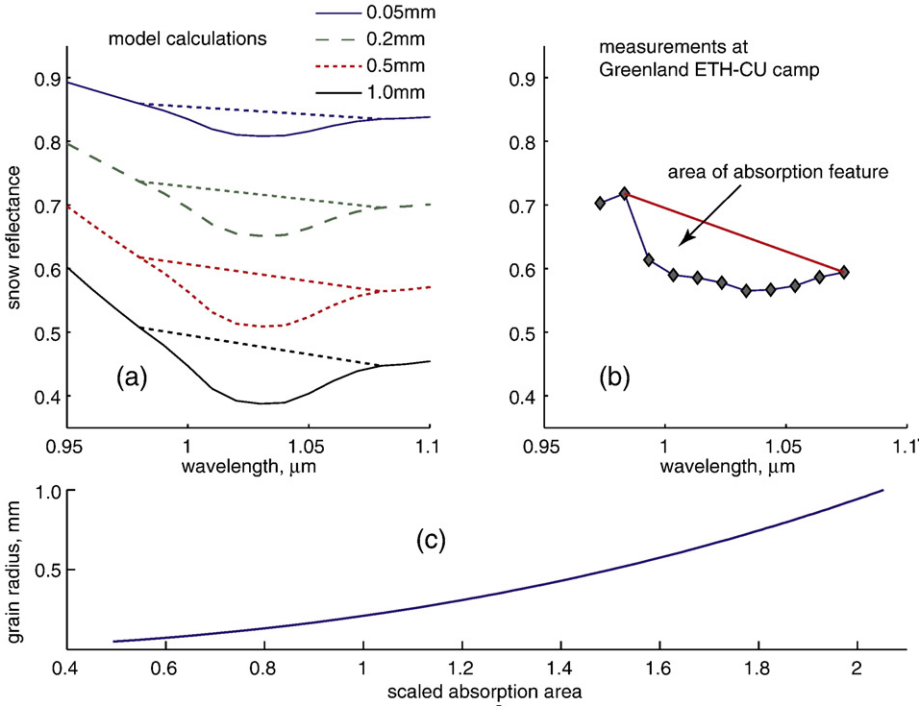

Fig. 6. (a) Theoretical relationship defining the scaled absorption area and showing its variability with grain size. (b) Field measurements from Greenland. (c) Relationship between grain size and scaled absorption area, showing how grain size can be estimated from measurements of the scaled absorption area with an imaging spectrometer.

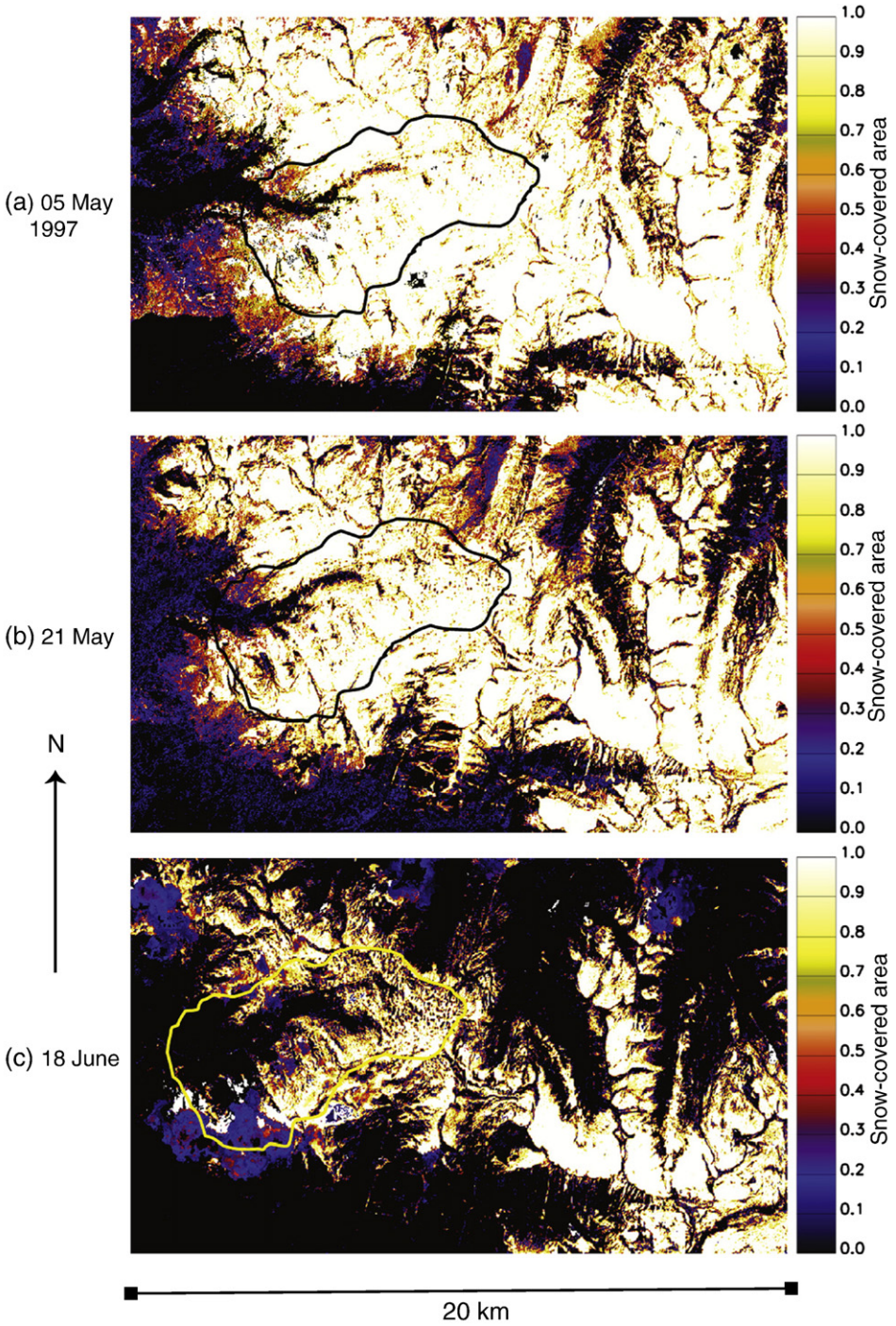

Fig. 7. Snow-covered area in the Tokopah Basin, Sierra Nevada, for three dates in the 1997 snowmelt season: (a) 05 May 1997, (b) 21 May, (c) 18 June.

(Roberts et al., 1998; Painter et al., 2003) is to cycle through a range of snow endmembers and choose the one that results in the lowest RMSE. In the case of snow, we consider a wide range of endmembers by modeling the spectral reflectance for the specific observation geometry for snow grain sizes from 10 μm, appropriate for clouds rather than snow, to 1200 μm, characteristic of very coarse spring snow. Fig. 7 shows the decline in snow-covered area, derived from AVIRIS data, for the Tokopah Basin in the Kaweah River drainage in the Sierra Nevada during the 1997 melt season. Fig. 8 shows the changes in grain size for the same period; the grain sizes are smaller in the middle image because of several small storms between 05 May and 21 May. These maps of fractional snow cover and grain size/albedo were used to drive a distributed snowmelt model discussed in a later section on Remotely sensed snow properties in hydrologic analyses.

2.4. Sensitivity to anisotropic reflectance

Painter and Dozier (2004) investigated the sensitivity of such spectral mixing to the anisotropic reflectance of snow. Retrievals of subpixel snow-covered area are progressively more sensitive to the HDRF (hemispherical-directional reflectance factor) as grain size decreases, solar zenith angle increases, and fractional snow cover

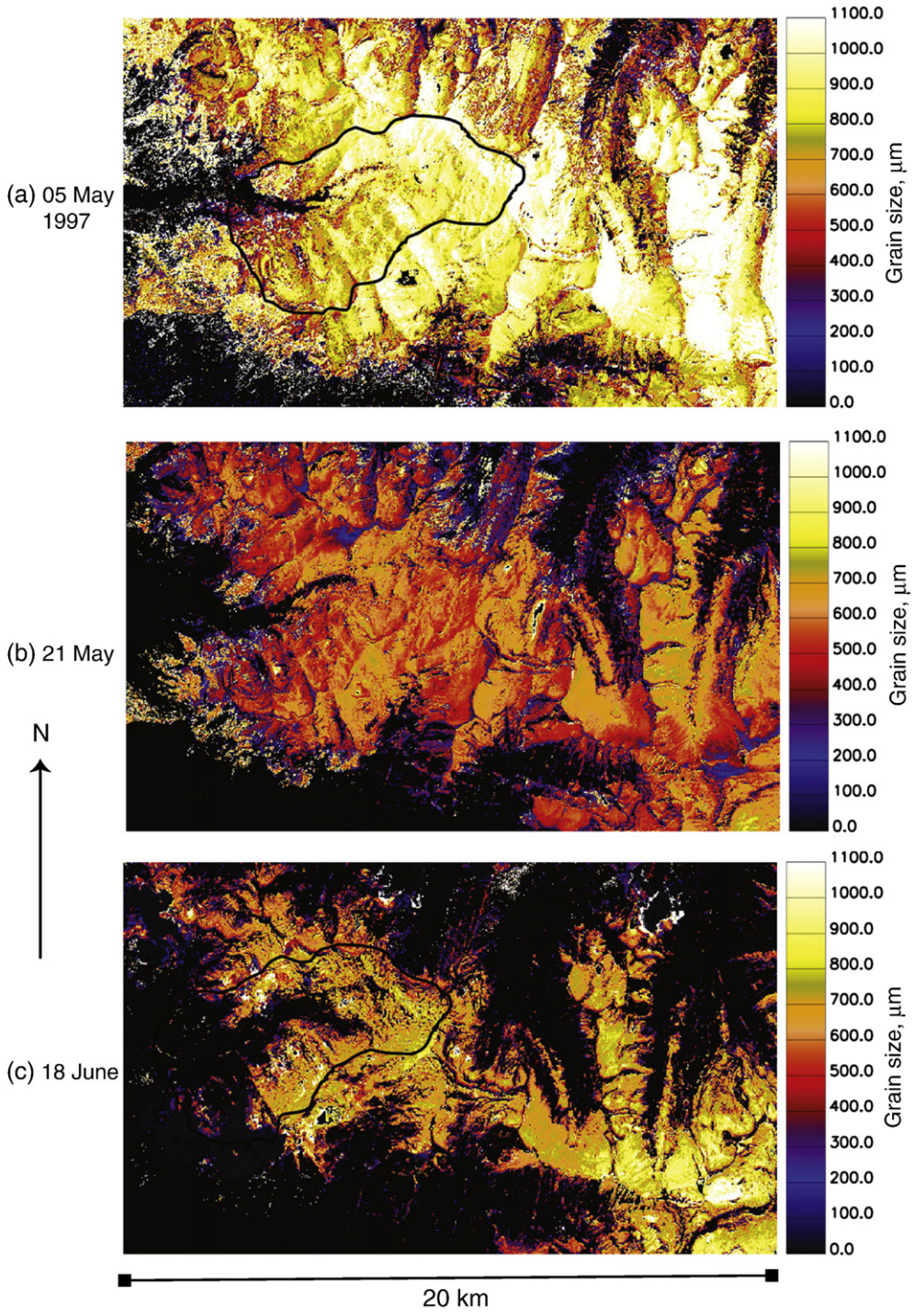

Fig. 8. Snow grain size for the snow-covered area images in Fig. 7: (a) 05 May 1997, (b) 21 May, (c) 18 June. Grain size became finer after the 05 May image because of several small storms.

increases. Spectral mixing overestimates snow cover in the forward reflectance angles by up to 20% and underestimates it in the backward reflectance angles by up to 15%. Grain size retrievals are more sensitive to anisotropy as grain size and solar zenith angle increase, but the retrievals of grain size are insensitive to snow-covered area. The largest inferred grain sizes are near a peak in the backward reflectance angles and the smallest generally occur at the largest viewing angles (from zenith) in the forward direction. Retrievals of albedo from both methods are similarly sensitive to anisotropy, with albedo errors up to 5% for a 30° solar zenith angle and up to 10% at 60°.

2.5. Liquid water

Remotely sensed images of snow also include atmospheric water vapor and may include liquid water too if the snow is melting. The basis for simultaneous measurement of all three phases of water resides in the spectroscopy of water in the solar spectrum, where each phase of water exhibits multiple absorption features between 0.4 and 2.5 µm. Water vapor exhibits finer spectral absorption structure because of the contribution of rotational absorption lines, whereas liquid water and ice exhibit the comparatively broad molecular absorption bands of

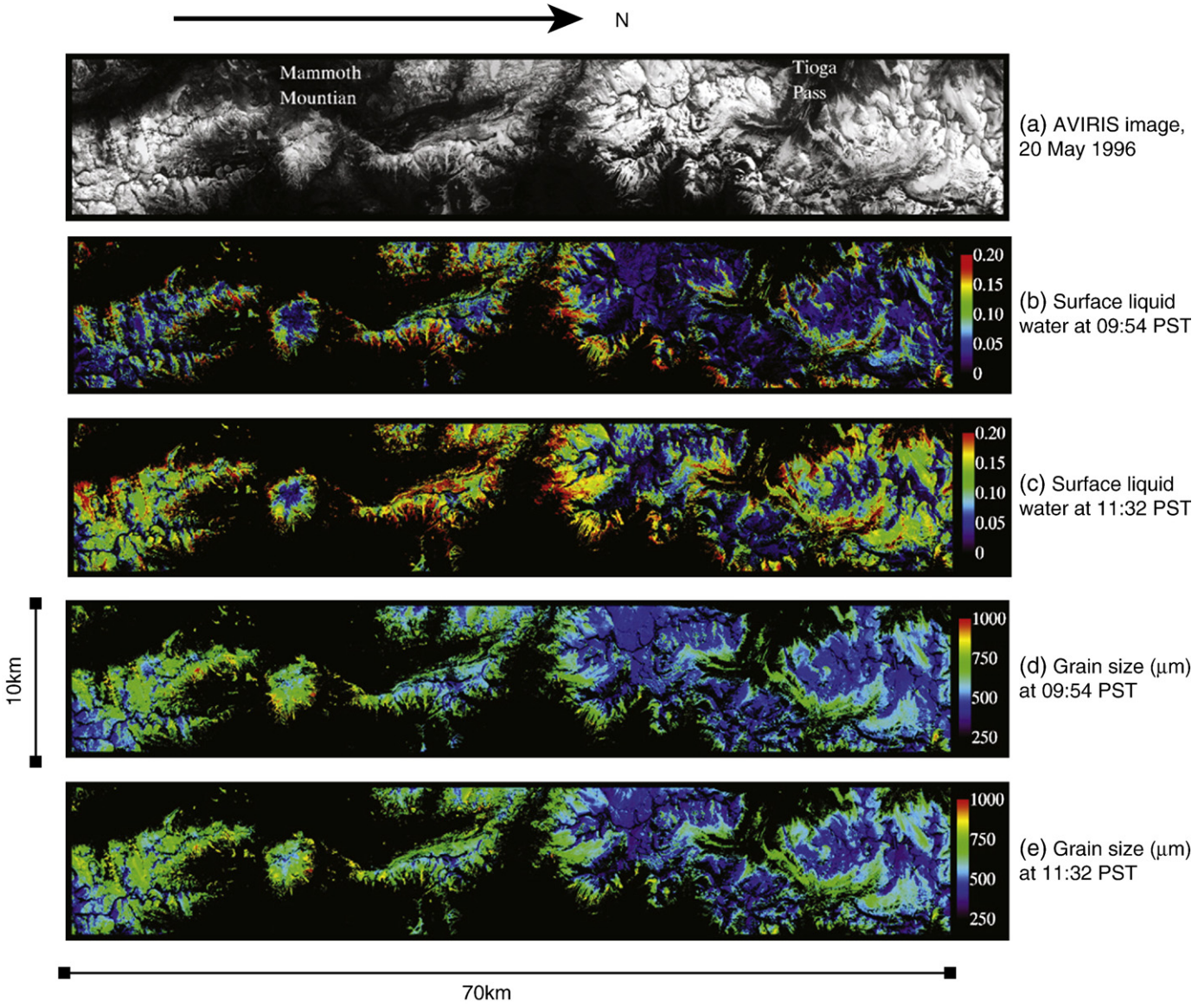

Fig. 9. (a) AVIRIS image of Sierra Nevada from south of Mammoth Mountain to north of Tioga Pass acquired on 20 May 1996. (b) Derived surface liquid water (0 to 0.20 volume fraction) at 09:54 PST (17:54 UTC). (c) Derived surface liquid water 98 min later, at 11:32 PST (19:32 UTC). (d) Derived grain size (radius of effective sphere, 250 to 1000 μm) at 09:54 PST. (e) Derived grain size at 11:32 PST.

liquid and solid compounds. In the spectral region from 0.85 to 1.1 μm, the absorption bands are of moderate strength and have absorption maxima at 0.94 μm for water vapor, 0.980 μm for liquid water, and 1.03 μm for water ice. This moderate absorption in conjunction with the spectral displacement provides spectroscopic leverage for decoupling and measuring the abundance of three phases of water from a single spectroscopic measurement (Green et al., 2006).

Fig. 9 shows the regional variability of grain size and liquid water using two AVIRIS data sets acquired 98 min apart over a 10 km × 70 km region of the Sierra Nevada on 20 May 1996. Snow grain size, expressed as the radius of an equivalent sphere, varied from 250 to 1000 μm; liquid water volume fraction varied from 0 to 0.20. To calculate the single-scattering optical properties of wet snow from the refractive indices of ice and water, we use a layered-sphere Mie code (Toon & Ackerman, 1981). Both coated-sphere and dispersed-sphere models might be appropriate to assess the radiative expression of liquid water in melting snow (Green et al., 2002), but we adopt the coated-sphere model as most closely matching our field reflectance measurements. It is possible that the dispersed-sphere model is more appropriate when the water content is low (Davis et al., 1987). The range and distribution of grain size and liquid water fraction are consistent with the expected status of the late spring snow pack, air temperature, and elevations of the region. At a high-altitude site on Mammoth Mountain, the derived grain size and liquid water fraction were 350 μm and 0.0. At a nearby low-altitude site, values of 650 μm and 0.13 were derived. The second data set acquired 98 min later showed a pronounced increase in liquid water throughout the study area consistent with the increased solar heating and air temperature at the later time. At the Tioga Pass summit, liquid water increased from 0.0 to 0.05; at the low-elevation site, liquid water increased from 0.13 to 0.18.

2.6. Dust and algae

AVIRIS data collected in the spring over two energy balance monitoring sites in the alpine and subalpine of Red Mountain Pass in the San Juan Mountains of Colorado show clearly the degraded albedo caused by dust from the Utah desert (Painter et al., 2007). Fig. 10 shows the concept of *radiative forcing,* comparing the net solar radiation of dirty vs. clean snow. Cassidy and Painter (2005) developed a scaled integral dust-impact index (SIDI) to estimate relative dust

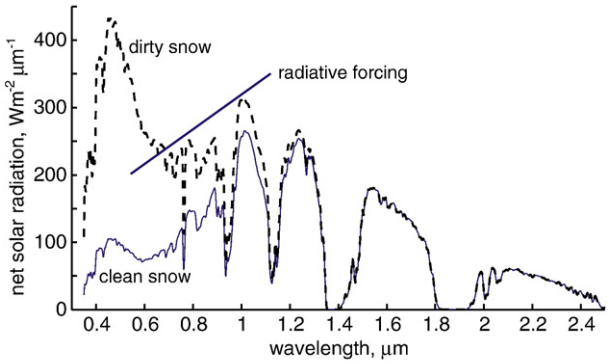

Fig. 10. Illustration of radiative forcing by dust. Net solar radiation curves for clean and dirty snow are derived by multiplying the albedo values in Fig. 5a with the incoming solar radiation values in Fig. 2a on a flat surface at solar zenith angle 48°.

concentration. First, the grain size is estimated from the ice absorption feature at 1.03 µm (described in the section on Snow albedo). From the grain size, the reflectance of clean snow in the visible wavelengths can be calculated, and the difference between the actual reflectance and the modeled clean-snow value is used to estimate dust concentration. Fig. 11 shows an image of grain sizes and an image showing the areas where the snow contains dust. A needed improvement in this analysis is incorporation of topographic correction; without it, diffuse irradiance on snow in the shadows or on oblique slopes can cause a negative SIDI value.

The effect of algae on snow reflectance is similar to that of dust but can be separated. Because cells of red algae (*Chlamydomonas nivalis*) absorb at specific wavelengths in regions indicative of carotenoids and chlorophylls a and b, the spectral signature of snow containing the algae is distinct. Spectra show carotenoid absorption in the wavelength range from 0.4 to 0.58 µm and chlorophyll a and b absorption in the wavelength range from 0.6 to 0.7 µm. The integral of the scaled chlorophyll a and b absorption feature varies with algal concentration, similarly to the way the scaled absorption feature around 1.03 µm varies with grain size (Nolin & Dozier, 2000). Painter et al. (2001) were thus able to derive algal concentrations in the Tioga Pass region of the Sierra Nevada from low-altitude AVIRIS data. Over a 5.5 km^2 region, the retrieved spatial distribution was consistent with visual observations made in the field. Average algal spatial biomass concentration was 3.3×10^{-5} kg m^{-2}.

3. Remotely sensed snow properties in hydrologic analyses

3.1. Use of snow-covered area and albedo in hydrologic models

Does the albedo of snow matter? A way to test this question rigorously is to run a distributed snowmelt model using accurate maps of the fractional snow-covered area and albedo and compare the results to a simpler model, for example one that uses a basin-wide albedo updated with a standard aging function.

Molotch et al. (2004) examined snow ablation from a grid-based distributed snowmelt model, using field data from extensive snow surveys during the melt season to initialize the model with a spatial distribution of snow water equivalence and then to test the model with subsequent surveys. The albedo estimated from three AVIRIS flights during the melt season typically differed by 20% from albedo estimated using a commonly used empirical relation based on the age of the snow (U.S. Army Corps of Engineers, 1956). In some parts of the basin, differences were as large as 31%. Using the AVIRIS albedo estimates in a distributed snowmelt model that explicitly includes spatially and temporally variable albedo resulted in a much more accurate estimate of the timing and magnitude of snowmelt as compared to the same model with the empirical albedo. The R^2 value, of modeled versus measured snowmelt, increased from 0.59 to 0.73 and the error magnitude decreased from 36% to 2%. Model improvement was most significant in areas and at times where incident solar radiation was relatively high and temperatures low.

The results showing that imaging spectrometry to retrieve liquid water in the surface layer are too recent to have been incorporated into hydrologic models. However, they demonstrate a consistent approach to the use of calibrated imaging spectrometry to measure and monitor snow properties at the local and regional scale with contiguous spectral and spatial sampling. These derived parameters can improve energy-balance and runoff models through assimilation of measured values to update and constrain calculations.

3.2. Adaptation of imaging spectrometer techniques to multispectral sensors

Multispectral sensors, such as Landsat and MODIS, provide data over wider swaths and at more frequent intervals than imaging spectrometers. From Landsat, the spatial resolution is 30 m at 16-day intervals, whereas the information from MODIS on either EOS-Terra or EOS-Aqua satellite is sampled at 500 m spatial resolution at daily intervals (however the MODIS viewing angle extends to 55° off-nadir, so pixels at the edge of the scan are elongated by a factor of 5 in the cross-track direction and a factor of 2 in the along-track direction). Particularly in the case of MODIS, a snow and albedo mapping algorithm must use the limited spectral information to estimate the subpixel snow properties. Fortunately, snow's spectral characteristics in the MODIS bands are separable from those of soil and vegetation

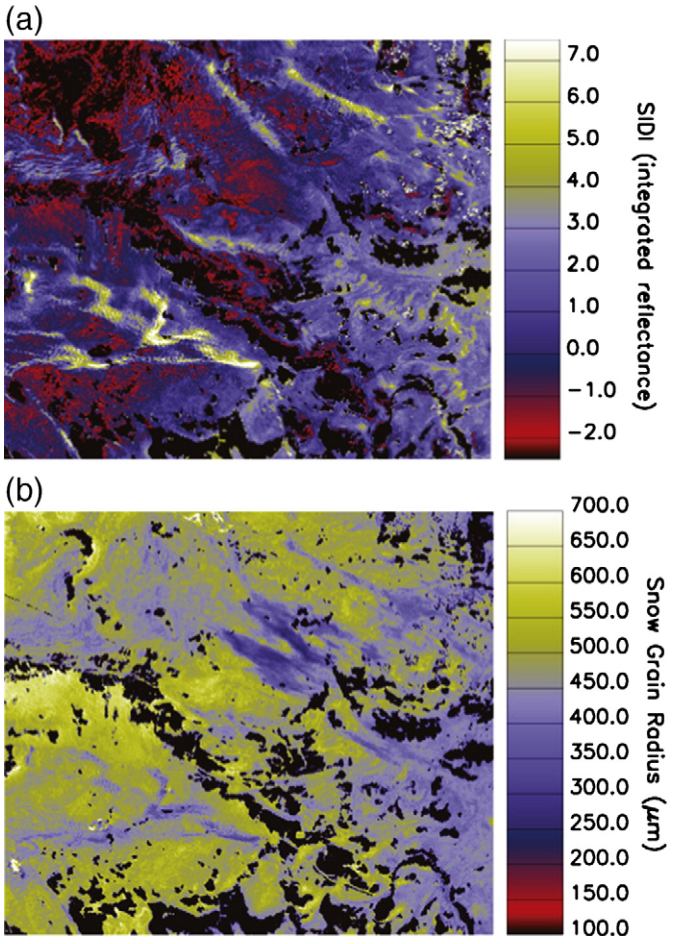

Fig. 11. AVIRIS images showing effect of dust on snow in the San Juan Mountains, Colorado: (a) radiative forcing caused by the confluence of areas of high incoming solar radiation and dirty snow, (b) grain size.

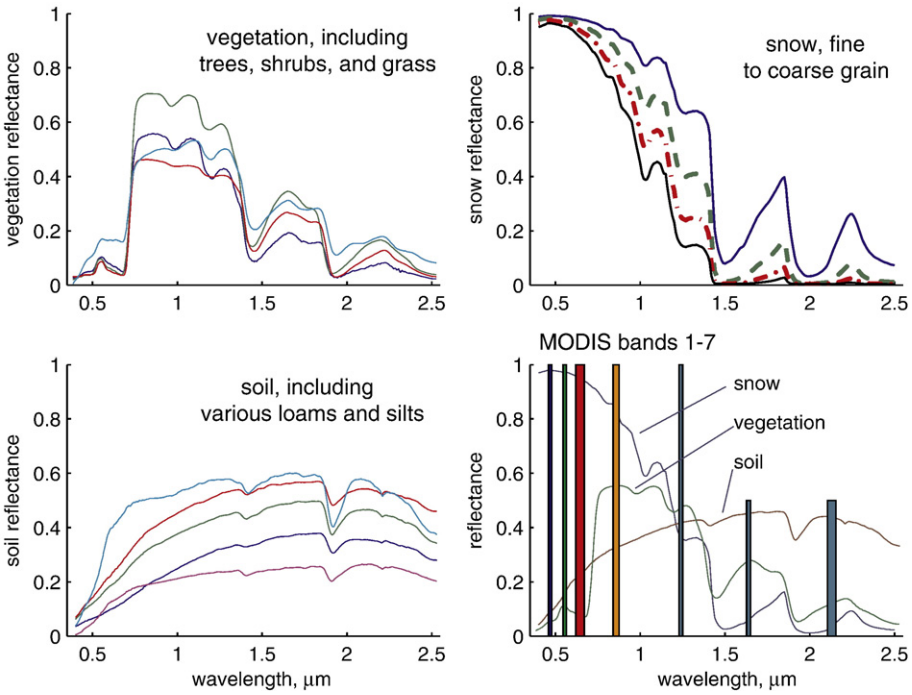

Fig. 12. Typical spectral reflectivity and variability for vegetation, soil, and snow. These surface covers are generally well separated in the MODIS bands.

(Fig. 12).The albedo measurements are necessary if a distributed energy-balance model is to use the snow properties as input.

We have adapted the multiple endmember spectral mixture analysis model (Painter et al., 2003), originally used with AVIRIS, to produce enhanced snow cover products from MODIS. The products include fractional snow cover within each 500 m pixel, plus the grain size and albedo of that fractional snow cover. The model is specifically aimed at providing an accurate estimate of snow cover for regional studies in mountainous areas anywhere but also applicable to polar and grassland regions. The model uses spectral libraries for snow endmembers generated with a radiative transfer model for varying grain size snow, adapted to the solar geometry of the specific scene.

Fig. 13 shows a MODIS image for the entire Sierra Nevada, along with the snow-covered area and grain size of that snow. With measurements of fractional snow covered area from 30 m Thematic Mapper data, we scale to 500 m to validate the MODIS retrievals (Fig. 14). These results show that the analysis with MODIS has regional mean errors in snow-covered area of −1% and standard deviations of 8%, compared to Landsat. However, these errors are partly caused by overestimation by the Thematic Mapper, because this sensor often saturates over pixels that are partly covered by snow.

4. Issues requiring further research

4.1. Variability of snow grain size with depth

In the surface layer of a snowpack, metamorphism can be complicated. Temperature gradients, and thus vapor gradients, during a diurnal cycle often switch directions in response to heating and cooling at the surface. Heating and cooling are asymmetric because solar radiation easily penetrates 5–10 cm into the snow, with some radiation reaching 50 cm, whereas the emitted longwave radiation is from the surface itself. Penetration of solar radiation is greatest in the visible part of the spectrum, especially for large grains, so if one

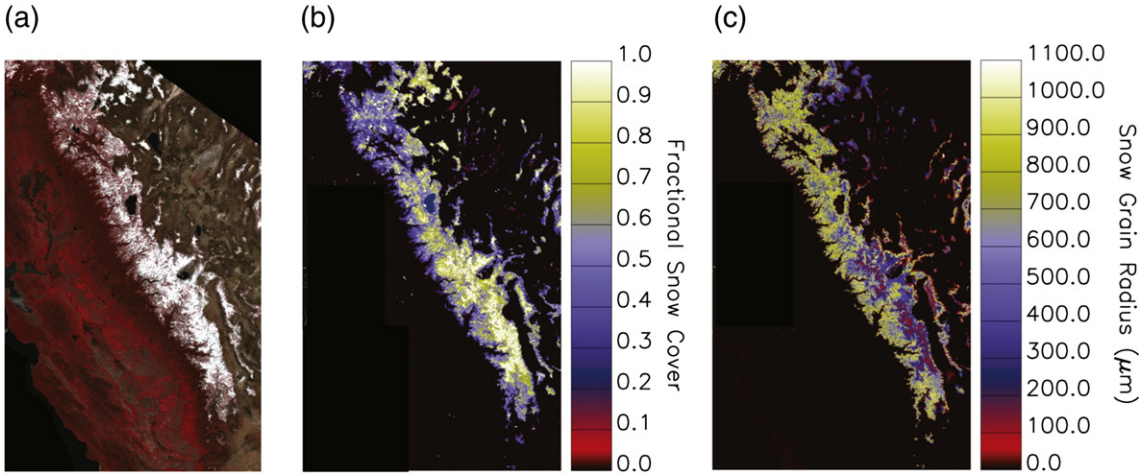

Fig. 13. (a) MODIS image of the Sierra Nevada, 07 March 2004, with RGB colors corresponding to wavelengths 0.858 μm, 0.645 μm, and 0.555 μm. (b) Fractional snow-covered area from that image. (c) Optically equivalent grain size.

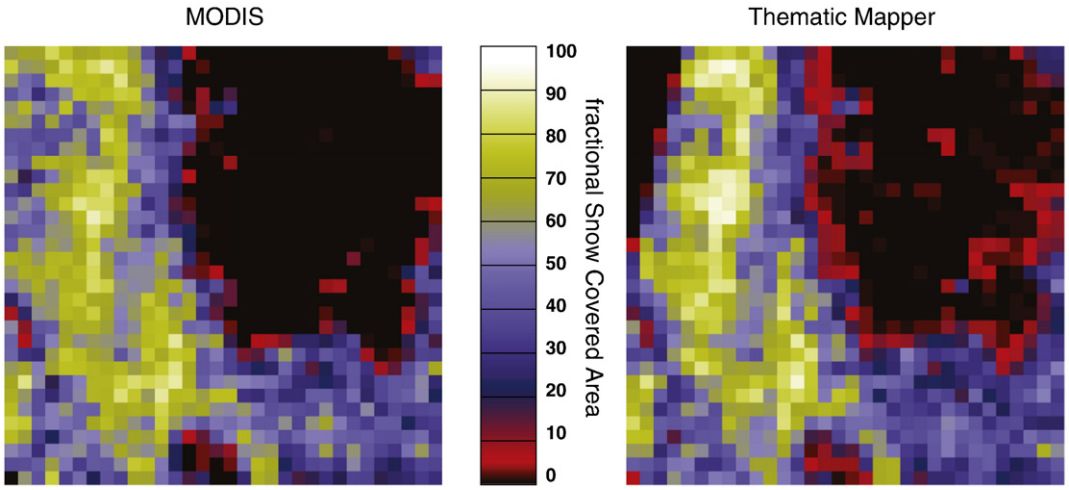

Fig. 14. Fractional snow-covered area from MODIS (500 m) and the Thematic Mapper (30 m) for a region covering the Rabbit Ears and North Park meso-cell study areas (25 km × 25 km) of the Cold Land Processes Experiment on April 4, 2002. The triangular void in upper left of the Thematic Mapper image is outside the image swath. These data demonstrate the spatial consistency and accuracy of estimating subpixel snow cover from MODIS.

assumes a single-layer (homogeneous) snow model, the retrieved snow grain size can appear to depend on wavelength (Li et al., 2001; Zhou et al., 2003).

Li et al. (2001) describe a retrieval of grain sizes over sea ice using AVIRIS data at wavelengths 0.86, 1.05, 1.24 and 1.73 μm. By calculating a spectral photon-penetration depth—defined as the *e*-folding flux attenuation depth—and assuming that grain size increases with depth, they are able to model a retrieval of the depth dependence of grain size. However, this assumption of greater grain size at depth is not always realistic— surface hoar layers often have a large grain size—and their model was not tested with field data. Nevertheless, the variability of grain size with depth does present an issue when calculating spectral albedo over all solar wavelengths based on estimates from a discrete set of wavelengths.

4.2. Angular effects: the basis for spectro-directional remote sensing of snow

Just as our eyes record information about both color and texture using reflected light, so do optical sensors. For nearly all land surface types, the variations of reflectance with viewing angle provide details about the structure and heterogeneity of the reflecting surface. Multi-angle viewing can tell us about the surface roughness and provides unique information not always present in spectral data. Spectro-directional remote sensing (Schaepman, 2007) combines both spectral and angular data to better characterize Earth's surface, including snow and ice. Using data from the Multi-angle Imaging SpectroRadiometer (MISR), Nolin et al. (2002) found that multi-spectral observations could not distinguish between smooth and crevassed glaciers in Antarctica because they were spectrally identical. However the smooth ice surface scattered in the forward direction, whereas the crevassed ice scattered more in the backward direction, making them readily distinguishable with multi-angular viewing. Similarly, Nolin and Payne (2007) combined albedo and surface roughness derived from multi-angular data to differentiate glacier zones in western Greenland.

With MISR data, Nolin (2004) showed that for snow overlain by vegetation, the pattern of reflectance with varying angle (the "angular signature") could be used to estimate forest density. Because the proportion of shadowed substrate (soil or snow) in the field-of-view changes with viewing angle, a spectro-directional approach possibly could help address one of the current problems for satellite-derived snow covered area: fractional snow cover estimates from spectral unmixing produce only the projected area of snow cover and do not incorporate any vegetation correction.

The use of multi-angular remote sensing for characterizing snow and ice represents a new paradigm in optical remote sensing. To date, anisotropic reflectance from snow and ice is noise, not signal, to be corrected before geophysical parameters can be derived. Now, rather than correcting for anisotropy, one may exploit its properties to gather unique information about snow or ice sheet properties.

4.3. Spectro–temporal combination of imaging spectrometer and multispectral sensor

In addition to the spectro–directional signature of snow, the spectro–temporal signature can yield valuable understanding of the evolution of the state of snow cover. Imaging spectrometry allows characterization of snow grain size, impurity concentration, albedo, and surface liquid content, all of which can vary hourly. Moreover, snow lies in regions of frequent and at times persistent cloud cover so imaging at a fine temporal resolution is also desirable. Because of swath widths and data rates, it is unlikely that we will soon combine both attributes in the same sensor.

In the next decade, it is likely that both an operational multi-spectral sensor and an imaging spectrometer will orbit simultaneously. The multispectral sensor, VIIRS (Visible/Infrared Imager/Radiometer Suite), will be available from NPP and NPOESS. NPOESS (National Polar Orbiting Environmental Satellite System) is the next generation operational set of satellites for climate and meteorology, scheduled for launch around 2013. The NPOESS Preparatory Project (NPP) is scheduled to launch in 2010.

As for an imaging spectrometer, among the 17 missions recommended by the recent "decadal survey" on Earth science from space by the National Research Council (2007) is HyspIRI, the Hyperspectral Infrared Imager. Although primarily designed to detect responses of ecosystems to land management and climate change, with a secondary objective to map surface rock and soil composition, HyspIRI would be suitable for the study of snow. Planned specifications include a spectrometer with 210 spectral bands covering the 0.4–2.5 μm region, along with a multispectral infrared sensor over 8–12 μm. Spatial resolution is 45 m, swath width is 90 km, and orbit repeat interval is 30 days but with pointing capability to image short-lived events if needed.

The issue for future research is to best use this synergistic data collection that combines fine spectral and spatial resolution (HyspIRI) with a broad swath and daily coverage of the whole Earth (VIIRS). The obvious application is to frequently test VIIRS data records with HyspIRI, but a more ambitious (and at this time, vague) task is to assimilate both

sets of observations with models of snow cover and albedo evolution. Current practice with daily MODIS data is to use spatial and temporal interpolation to correct for cloud cover and viewing angle and thereby estimate the fractional snow cover and albedo for each pixel for each day of the snow season (Dozier et al., 2008). The adaptation of these methods to include multiple sensors and models is a worthwhile challenge for the immediate future.

4.4. Planetary snow and imaging spectrometry

Imaging spectrometers are flying on current planetary missions and planned for a future lunar mission. CRISM (Compact Reconnaissance Imaging Spectrometer for Mars) was launched on the Mars Reconnaissance Observer (MRO) in August 2005 and began collecting data in September 2006 (CRISM, 2007). Spanning the spectral region from 0.362 to 3.92 μm at 6.55 nm resolution, CRISM is designed mainly to look for trace minerals left behind when water evaporates and thereby reveal Mars' past wet environments, including seasonal snow and snowmelt (Russell & Head, 2007). The instrument will also watch seasonal variations in Martian snow—composed mainly of frozen CO_2 grains where frozen H_2O is an impurity, as is dust (Warren et al., 1990; Nolin, 1998). The instrument has a fine enough spectral resolution to detect liquid water in snow (Green et al., 2006), as discussed in the earlier section on Liquid water. Water might occur locally where absorption by the dust raises the temperature. Moreover, the measurements would enable a similar analysis of radiative forcing by dust (Painter et al., 2007) that is discussed in the earlier section on Dust and algae.

VIMS (Visible and Infrared Mapping Spectrometer) on Cassini is collecting data from Saturn and its moons at wavelengths from 0.3 to 5.1 μm (Cassini VIMS, 2006). Results so far include identification of water ice on several of the satellites (Filacchione et al., 2007), along with ice mixed with impurities on Titan (McCord et al., 2006).

The Moon Mineralogy Mapper (M^3) is one of two instruments that NASA is contributing to India's first mission to the Moon, Chandrayaan-1, which launched in October 2008 (Moon Mineralogy Mapper, 2007). M^3 covers the spectral range 0.43 to 3.0 μm and will provide the first map of the entire lunar surface at high spatial and spectral resolution. One of the goals is to look for the putative ice in the permanently shaded polar craters.

4.5. Routine use of remotely sensed snow measurements in models of hydrology and climate

Independent ground-based observations have long supported operational management of the snowmelt water resource and regional-scale climate modeling (NOAA, 2003), yet they leave much of the snowpack poorly sampled. Owing to complex topography and heterogeneous snow and vegetation cover, research is clearly needed to develop hydrologic network designs that, together with advances in modeling and remote sensing, would better characterize the fluxes and reservoirs in the mountains, and provide necessary information on large-scale partitioning of snowmelt between runoff, infiltration, sublimation, and evapotranspiration. Such new integrated observations would enhance decision support systems by more densely sampling the range of changes and responses considered and by reducing prediction uncertainties (Bales et al., 2006).

Remote sensing is the only practical way to measure the spatial extent and variability of snow cover and albedo. Because alpine terrain often varies at a spatial scale finer than that of the ground instantaneous field of view of the remote sensing instrument, this heterogeneity requires that we map snow-covered area and snow albedo at subpixel resolution in order to accurately represent its spatial distribution. Otherwise, systematic errors result. While overestimates may balance underestimates for the basin average, distributed hydrologic applications in mountainous regions require the spatial distribution of snow cover.

Because the optical wavelengths cannot measure depth or snow water equivalent, and lacking a microwave instrument that can measure these variables in the mountains, there remains a pressing research need to develop strategies to blend remotely sensed and ground-based data, including measurement network design, to accurately estimate snow water equivalent (Bales et al., 2006).

5. Conclusion

Among natural materials at Earth's surface, snow has a huge range of spectral reflectance values depending on its physical characteristics, primarily the grain size but also dust or soot content, organic substances such as algae, and liquid water. Understanding this variability is important because more than one billion people depend on melting snow or glaciers for their primary water resource. In the last three decades, we have seen a productive coupling between better measurements and models of the optical properties of snow and advances in remote sensing. Foremost among these has been the use of data from imaging spectrometers to interpret snow properties. The important properties we can measure are: fractional snow-covered area, grain size (expressed as the sphere with equivalent surface-to-volume ratio), liquid water content in the near-surface layer, concentration of snow algae, and radiative forcing caused by dust. From grain size and other impurities, spectral and broadband albedo can be estimated. All of these results with imaging spectrometry (applied to snow on Earth) have been verified with surface measurements or, in the case of fractional snow-covered area, with high-resolution aerial photography.

Because snow varies temporally and because imaging spectrometer data are seldom available as seasonal time series, algorithms and practices have propagated to multispectral sensors, with the result of improved snow products from MODIS. The remaining challenges are to improve snow mapping in forests, adapt to angular variability in the signal, further investigate the measurement and consequences of absorbing impurities in snow, and incorporate information from both operational sensors and imaging spectrometers into hydrologic models.

Acknowledgments

The work is supported by NASA Cooperative Agreement NNG04GC52A, NASA Grant NNG04GL95G, NSF Grants EAR-0537327 and ATM-0432327, and the MISR Science Team. Part of this work was preformed at the Jet Propulsion Laboratory, California Institute of Technology under a contract with the NASA. We are grateful to Gregg Vane for comments on imaging spectrometry in the planetary context.

References

Bales, R. C., Molotch, N. P., Painter, T. H., Dettinger, M. D., Rice, R., & Dozier, J. (2006). Mountain hydrology of the western United States. *Water Resources Research*, *42*, W08432. doi:10.1029/2005WR004387.

Cassidy, M. P., & Painter, T. H. (2005). Hyperspectral analysis of dust concentration, snow grain size, and broadband albedo of alpine snowcover. *Eos, Transactions American Geophysical Union*, *86*(52) (Fall Meeting Supplement, Abstract C21A-1056).

Cassini VIMS. (2006). *Science Investigations.* (http://wwwvims.lpl.arizona.edu/).

Colbeck, S. C. (1979). Grain clusters in wet snow. *Journal of Colloid and Interface Science*, *72*(3), 371–384.

CRISM (2007). *Compact Reconnaissance Imaging Spectrometer for Mars.* (http://crism.jhuapl.edu/).

Davis, R. E., Dozier, J., & Chang, A. T. C. (1987). Snow property measurements correlative to microwave emission at 35 GHz. *IEEE Transactions on Geoscience and Remote Sensing*, *25*(6), 751–757.

Dozier, J., & Painter, T. H. (2004). Multispectral and hyperspectral remote sensing of alpine snow properties. *Annual Review of Earth and Planetary Sciences*, *32*, 465–494. doi:10.1146/annurev.earth.32.101802.120404.

Dozier, J., Painter, T. H., Rittger, K., & Frew, J. E. (2008). Time-space continuity of daily maps of fractional snow cover and albedo from MODIS. *Advances in Water Resources*, *31*, 1515–1526. doi:10.1016/j.advwatres.2008.08.011.

Filacchione, G., Capaccioni, F., McCord, T. B., Coradini, A., Cerroni, P., Bellucci, G., et al. (2007). Saturn's icy satellites investigated by Cassini-VIMS-I. Full-disk properties: 350–5100 nm reflectance spectra and phase curves. *Icarus*, *186*(1), 259–290. doi:10.1016/j.icarus.2006.08.001.

Flanner, M. G., & Zender, C. S. (2006). Linking snowpack microphysics and albedo evolution. *Journal of Geophysical Research*, *111*, D12208. doi:10.1029/2005JD006834.
Gao, B. C., & Goetz, A. F. H. (1990). Column atmospheric water vapor and vegetation liquid water retrievals from airborne imaging spectrometer data. *Journal of Geophysical Research*, *95*(D4), 3549–3564. doi:10.1029/89JD02729.
Green, R. O. (2001). Atmospheric water vapor sensitivity and compensation requirement for Earth-looking imaging spectrometers in the solar-reflected spectrum. *Journal of Geophysical Research*, *106*(D15), 17443–17452. doi:10.1029/2000JD900799.
Green, R. O., Dozier, J., Roberts, D. A., & Painter, T. H. (2002). Spectral snow reflectance models for grain size and liquid water fraction in melting snow for the solar reflected spectrum. *Annals of Glaciology*, *34*, 71–73.
Green, R. O., Eastwood, M. L., Sarture, C. M., Chrien, T. G., Aronsson, M., Chippendale, B. J. et al (1998). Imaging spectroscopy and the Airborne Visible Infrared Imaging Spectrometer (AVIRIS). *Remote Sensing of Environment*, *65*(3), 227–248. doi:10.1016/S0034-4257(98)0064-9.
Green, R. O., Painter, T. H., Roberts, D. A., & Dozier, J. (2006). Measuring the expressed abundance of the three phases of water with an imaging spectrometer over melting snow. *Water Resources Research*, *42*, W10402. doi:10.1029/2005WR004509.
Grenfell, T. C., & Warren, S. G. (1999). Representation of a nonspherical ice particle by a collection of independent spheres for scattering and absorption of radiation. *Journal of Geophysical Research*, *104*(D24), 31697–31709.
Gueymard, C. A. (2004). The sun's total and spectral irradiance for solar energy applications and solar radiation models. *Solar Energy*, *76*(4), 423–453. doi:10.1016/j.solener.2003.08.039.
Li, W., Stamnes, K., Chen, B. Q., & Xiong, X. (2001). Snow grain size retrieved from near-infrared radiances at multiple wavelengths. *Geophysical Research Letters*, *28*(9), 1699–1702.
McCord, T. B., Hansen, G. B., Buratti, B. J., Clark, R. N., Cruikshank, D. P., D'Aversa, E., et al. (2006). Composition of Titan's surface from Cassini VIMS. *Planetary and Space Science*, *54*(15), 1524–1539. doi:10.1016/j.pss.2006.06.007.
Molotch, N. P., & Bales, R. C. (2006). Comparison of ground-based and airborne snow surface albedo parameterizations in an alpine watershed: Impact on snowpack mass balance. *Water Resources Research*, *42*, W05410. doi:10.1029/2005WR004522.
Molotch, N. P., Painter, T. H., Bales, R. C., & Dozier, J. (2004). Incorporating remotely sensed snow albedo into spatially distributed snowmelt modeling. *Geophysical Research Letters*, *31*, L03501. doi:10.1029/2003GL019063.
Moon Mineralogy Mapper (2007), http://moonmineralogymapper.jpl.nasa.gov/.
National Research Council (2007). *Earth science and applications from space: National imperatives for the next decade and beyond.*Washington D.C.: National Academies Press (400 pp.).
NOAA (2003), National snow analyses, http://www.nohrsc.nws.gov/products.html
Nolin, A. W. (1998). Mapping the Martian polar ice caps: Applications of terrestrial optical remote sensing methods. *Journal of Geophysical Research*, *103*(E11), 25851–25864. doi:10.1029/98JE02082.
Nolin, A. W. (2004). Towards retrieval of forest cover density over snow from the Multi-angle Imaging SpectroRadiometer (MISR). *Hydrological Processes*, *18*, 3623–3636. doi:10.1002/hyp.5803.
Nolin, A. W., & Dozier, J. (2000). A hyperspectral method for remotely sensing the grain size of snow. *Remote Sensing of Environment*, *74*(2), 207–216. doi:10.1016/S0034-4257(00)00111-5.
Nolin, A. W., Dozier, J., & Mertes, L. A. K. (1993). Mapping alpine snow using a spectral mixture modeling technique. *Annals of Glaciology*, *17*, 121–124.
Nolin, A. W., Fetterer, F. M., & Scambos, T. A. (2002). Surface roughness characterizations of sea ice and ice sheets: Case studies with MISR data. *IEEE Transactions on Geoscience and Remote Sensing*, *40*(7), 1605–1615. doi:10.1109/TGRS.2002.801581.
Nolin, A. W., & Payne, M. (2007). Classification of glacier zones in western Greenland using albedo and surface roughness from the Multi-angle Imaging SpectroRadiometer (MISR). *Remote Sensing of Environment*, *107*, 264–275. doi:10.1016/j.rse.2006.11.004.
Painter, T. H., Barrett, A. P., Landry, C., Neff, J., Cassidy, M. P., Lawrence, C., et al. (2004). Impact of disturbed desert soils on duration of mountain snowcover. *Geophysical Research Letters*, *31*, L12502. doi:10.1029/2007GL030284R.
Painter, T. H., & Dozier, J. (2004). The effect of anisotropic reflectance on imaging spectroscopy of snow properties. *Remote Sensing of Environment*, *89*(4), 409–422. doi:10.1016/j.rse.2003.09.007.
Painter, T. H., Dozier, J., Roberts, D. A., Davis, R. E., & Green, R. O. (2003). Retrieval of subpixel snow-covered area and grain size from imaging spectrometer data. *Remote Sensing of Environment*, *85*(1), 64–77. doi:10.1016/S0034-4257(02)00187-6.
Painter, T. H., Duval, B., Thomas, W. H., Mendez, M., Heintzelman, S., & Dozier, J. (2001). Detection and quantification of snow algae with an airborne imaging spectrometer. *Applied and Environmental Microbiology*, *67*(11), 5267–5272. doi:10.1128/AEM.67.11.5267-5272.2001.
Pearlman, J. S., Barry, P. S., Segal, C. C., Shepanski, J., Beiso, D., & Carman, S. L. (2003). Hyperion, a space-based imaging spectrometer. *IEEE Transactions on Geoscience and Remote Sensing*, *41*(6), 1160–1173. doi:10.1109/TGRS.2003.815018.
Roberts, D. A., Gardner, M., Church, R., Ustin, S. L., Scheer, G., & Green, R. O. (1998). Mapping chaparral in the Santa Monica Mountains using multiple endmember spectral mixture models. *Remote Sensing of Environment*, *65*(3), 267–279. doi:10.1016/S0034-4257(98)00037-6.
Russell, P. S., & Head, J. W. (2007). The Martian hydrologic system: multiple recharge centers at large volcanic provinces and the contribution of snowmelt to outflow channel activity. *Planetary and Space Science*, *55*(3), 315–332. doi:10.1016/j.pss.2006.03.010.
Sabol, D. E., Jr., Adams, J. B., & Smith, M. O. (1992). Quantitative subpixel spectral detection of targets in multispectral images. *Journal of Geophysical Research*, *97*(E2), 2659–2672.
Schaepman, M. (2007). Spectrodirectional remote sensing: from pixels to processes. *International Journal of Applied Earth Observation and Geoinformation*, *9*(2), 204–223. doi:10.1016/j.jag.2006.09.003.
Stroeve, J., Box, J. E., Gao, F., Liang, S., Nolin, A., & Schaaf, C. (2005). Accuracy assessment of the MODIS 16-day albedo product for snow: Comparisons with Greenland in situ measurements. *Remote Sensing of Environment*, *94*(1), 46–60. doi:10.1016/j.rse.2004.09.001.
Toon, O. B., & Ackerman, T. P. (1981). Algorithms for the calculation of scattering by stratified spheres. *Applied Optics*, *20*(20), 3657–3660.
U.S. Army Corps of Engineers (1956). *Snow hydrology: Summary report of the snow investigations.*Portland, OR: North Pacific Division, Corps of Engineers (462 pp.).
Warren, S. G. (1982). Optical properties of snow. *Reviews of Geophysics and Space Physics*, *20*(1), 67–89.
Warren, S. G., & Wiscombe, W. J. (1980). A model for the spectral albedo of snow, II, Snow containing atmospheric aerosols. *Journal of the Atmospheric Sciences*, *37*(12), 2734–2745.
Warren, S. G., Wiscombe, W. J., & Firestone, J. F. (1990). Spectral albedo and emissivity of CO_2 in Martian polar caps—Model results. *Journal of Geophysical Research*, *95*(B9), 14717–14741. doi:10.1029/90JB00155.
Wiscombe, W. J. (2005). *Refractive indices of ice and water.* (ftp://climate1.gsfc.nasa.gov/wiscombe/).
Wiscombe, W. J., & Warren, S. G. (1980). A model for the spectral albedo of snow, I, Pure snow. *Journal of the Atmospheric Sciences*, *37*(12), 2712–2733.
Zhou, X., Li, S., & Stamnes, K. (2003). Effects of vertical inhomogeneity on snow spectral albedo and its implication for optical remote sensing of snow. *Journal of Geophysical Research*, *108*(D23), 4738. doi:10.1029/2003JD003859.